Biochemical Pharmacology 230 (2024) 116611

Contents lists available at ScienceDirect

Biochemical Pharmacology

journal homepage: www.elsevier.com/locate/biochempharm

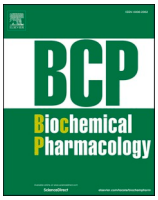

Regulatory roles of histamine receptor in astrocytic glutamate clearance under conditions of increased glucose variability

Yu Zhou [a,1], Wenhuo Xie [a,1], Chenghua Kong [a], Wei Luo [b], Hong Wei [c,*], Jiaping Zheng [b,*]

[a] Department of Clinical Pharmacy and Pharmacy Administration, School of Pharmacy, Fujian Medical University, Fuzhou, China
[b] Department of Rehabilitation Medicine, School of Health, Fujian Medical University, Fuzhou, China
[c] Shengli Clinical Medical College of Fujian Medical University, Cadres's Healthcare Office, Fujian Provincial Hospital, Fuzhou University Affiliated Provincial Hospital, Fuzhou, China

ARTICLE INFO

Keywords:
Diabetes
Glucose variability
Glutamate neurotoxicity
Histamine receptor
Mitochondrial function

ABSTRACT

In diabetic patients, repeated episodes of hypoglycemia can increase glucose variability (GV), which may lead to glutamate neurotoxicity in the brain and consequently affect cognitive functions. Astrocytes play a crucial role in regulating the balance of glutamate within the brain, and their function is influenced by the histamine receptor (HR) signaling pathway. However, the specific role of this mechanism under conditions of high GV is not yet clear. The results showed that increased GV resulted in decreased expression of HRs in mice hippocampus and astrocytes cultured in vitro. Additionally, a decrease in the expression of proteins related to glutamate metabolic clearance was observed, accompanied by a reduction in glutamate reuptake capacity. Notably, the intervention with histidine/histamine was able to reverse the above changes. Further mechanistic studies showed that inhibition of HRs that increased GV led to significant disturbances in astrocytic mitochondrial function. These abnormalities encompassed increased fragmentation morphology and the accumulation of reactive oxygen species, accompanied by decreased mitochondrial respiratory capacity and dysregulation of dynamics. Distinct HR subtypes exhibited variations in the modulation of mitochondrial function, with H_3R demonstrating the most pronounced impact. The overexpression of H_3R could enhance glutamate metabolic by reversing disturbances in mitochondrial dynamics. Therefore, this study suggests that H_3R is able to maintain glutamate metabolic clearance capacity and exert neuroprotective effects in astrocytes that increased GV by regulating mitochondrial dynamic balance. This provides an important basis for potential therapeutic targets for diabetes-related cognitive dysfunction.

1. Introduction

Glucose variability (GV) refers to the condition of instability characterized by fluctuations in blood glucose levels between high and low values, which serves as a critical indicator for evaluating glycemic control in patients with diabetes [1]. Diabetic patients often experience increased GV due to hypoglycemic events during treatment and subsequent reactive hyperglycemia [2]. Research shows that although frequent non-severe hypoglycemic events are not directly life-threatening, the resulting high GV can lead to a decline in cognitive function [3–5] and is considered an independent risk factor for complications in diabetic patients [2,6]. Our previous study revealed that

Abbreviations: GV, glucose variability; HR, histamine receptor; ROS, reactive oxygen species; RT-qPCR, real time quantitative PCR; GFP, green fluorescent protein; MOI, multiplicity of infection; ADP, adenosine diphosphate; ATP, adenosine triphosphate; OCR, oxygen consumption rate; Ct, cycle threshold; ANOVA, one-way analysis of variance; GFAP, glial fibrillary acidic protein; GLAST, glutamate-aspartate transporter; GLT-1, glutamate transporter-1; GS, glutamate synthetase; DHAP, dihydroxyacetone phosphate; TCA, tricarboxylic acid; cAMP, cyclic adenosine monophosphate; mtDNA, mitochondrial DNA; DRP1, dynamin-related protein 1; MFN2, mitofusin-2; OPA1, optical atrophy 1; T1D, type 1 diabetic; MAPK, mitogen-activated protein kinase; STZ, streptozotocin; DMEM, dulbecco's modified eagle medium; FBS, fetal bovine serum; OD, optical density; HBSS, Hank 's balanced salt solution; FCCP, carbonyl cyanide phosphor-(p)-trifluoromethoxy phenylhydrazone; PCA, principal component analysis. MCC, Manders' Colocalization Coefficients; DAPI, 4,6-diamino-2-phenyl indole; PBS, phosphate buffered saline; DG, deoxyglucose; NAD, nicotinamide adenine dinucleotide; NC, normal control; NG, normal glucose.

* Corresponding authors.
E-mail addresses: fjphwh1688@163.com (H. Wei), zhengjp@fjmu.edu.cn (J. Zheng).
[1] These authors contributed equally to this work contributed equally to this work.

https://doi.org/10.1016/j.bcp.2024.116611
Received 26 July 2024; Received in revised form 26 September 2024; Accepted 4 November 2024
Available online 5 November 2024

the detrimental effects of increased GV on cognitive function stemmed from the intricate interplay between hyper- and hypoglycemic interactions, rather than mere superimposition [7,8]. However, effective preventive or therapeutic strategies for cognitive impairment resulting from increased GV induced by recurrent hypoglycemia are still lacking.

Astrocytes, the most abundant glial cell type in the central nervous system, play a crucial role in regulating neuronal network activity, synaptogenesis, and supporting cognitive processes [9]. This effect is largely dependent on its maintenance of the metabolic balance of glutamate, the major excitatory neurotransmitter [10]. Studies have demonstrated that the presence of glutamate toxicity in cognitive brain regions associated with insulin-induced hypoglycemia and diabetes [11–13]. Moreover, mounting evidence suggests that mitochondria play a pivotal role in the uptake and transformation of glutamate within astrocytes [14]. It has been observed that the energy metabolism pattern of mitochondria in human-derived astrocytes undergoes alteration under conditions of recurrent hypoglycemia in vitro, characterized by increased fatty acid oxidation and decreased energy coupling efficiency [15]. Likewise, mouse primary astrocytes exhibit decreased mitochondrial membrane potential, heightened levels of reactive oxygen species (ROS), and reduced maximal and reserve respiratory capacity following recurrent hypoglycemia with subsequent hyperglycemia [16]. These alterations can be reversed by the addition of the mitochondria-targeted antioxidant SS-31, thereby restoring astrocyte function [16]. Hence, a thorough investigation into mitochondrial function in astrocytes and its impact on the balance of glutamate metabolism is crucial for comprehending the mechanism underlying cognitive impairment induced by increased GV, as well as for the development of novel intervention strategies.

Histamine, serving as a pivotal central neurotransmitter, maintains a close association with learning, memory, and energy metabolism. It is primarily synthesized by histaminergic neurons situated in the hypothalamus, projecting extensively throughout the brain [17]. Currently, four histamine receptors (HR) are known to exist in the brain, three of which (H_1R, H_2R, H_3R) are significantly expressed in astrocytes [17]. These receptors function by regulating various aspects of astrocyte activity, including the removal of excess glutamate, modulation of signal transduction, maintenance of glucose metabolism balance, and stimulation of the release of neurotrophic factors [18]. Our previous research found that in mice under conditions of high GV, there were abnormalities in histidine metabolism in brain regions associated with cognition; by supplementing histidine (a precursor of histamine), it was possible to alleviate cognitive impairments caused by high GV, a process that involved varying degrees of activation of different subtypes of HRs [8]. These results indicate the involvement of histamine and its receptor system in alterations in brain cognitive function induced by increased GV. However, the specific effects of histamine on astrocytes and their regulatory mechanisms remain unclear.

Building upon prior research, the objective of this study is to delve deeper into how HR subtypes modulate the capacity of astrocytes to clear glutamate and to explore the essential mitochondrial pathways implicated in the induction of high GV by recurrent hypoglycemia. First, we established a mouse model simulating high GV conditions to observe changes in HR expression and metabolism in hippocampus. This was followed by in vitro studies using primary cultured astrocytes exposed to alternating high and low glucose conditions, mimicking the high GV environment. We then investigated the effects of histamine intervention and specific HR subtype inhibition on astrocyte function, particularly focusing on glutamate clearance. To elucidate the underlying mechanisms, we examined mitochondrial function, including ROS production, respiratory capacity, and dynamics. Finally, we conducted overexpression experiments targeting H_3R to confirm its role in regulating mitochondrial function and glutamate clearance.

2. Research design and methods

2.1. Animals

Male C57BL/6J mice (weighing 20–25 g) were purchased from Shanghai SLAC Laboratory Animal Co, Ltd., China. Each five mice shared a cage, and all mice had free access to food and water under 12 h light/12 h dark conditions. Animals were allowed to habituate to the novel environment for 1 week before performing any experimental manipulation. All animal experimental protocols were approved by the Animal Ethics Committee of Fujian Medical University to ensure that the study followed strict ethical guidelines, respected animal welfare, and minimized discomfort and suffering of animals.

2.2. Reagents

Reagents used are detailed in the Table 1. Antibodies and dilutions used for immunoblotting and immunofluorescence, as well as primers used for real time quantitative PCR (RT-qPCR) are listed in the Table 2, Table 3 **and** Table 4, respectively.

Table 1
Reagents used in this study.

Reagents	Reference	Company, Country
STZ	S0130	Sigma, USA
L-histidine	H8000	Sigma, USA
Hiatamine	V900396	Sigma, USA
Pyrilamine	P5514	Sigma, USA
Cimetidine	C4522	Sigma, USA
Thioperamide	T123	Sigma, USA
Glutamate test kit	MAK004-1KT	Sigma, USA
Glucose Uptake Assay Kit	MAK083-1KT	Sigma, USA
Insulin glargine	Lantus	Sanofi-Aventis, France
Regular insulin	N/A	Wanbang, China
MFI8	HY-150031	MCE, USA
DMEM	11885084/ 11966025	Gibco, USA
Trypsin-EDTA (0.25 %)	25,200,114	Gibco, USA
FBS	ST30-2602	Pansera ES, Germany
Glucose (20 %)	ST491	Beyotime Biotechnology, China
Hoechst 33,342	C1027	Beyotime Biotechnology, China
DAPI	C1002	Beyotime Biotechnology, China
Mito-Tracker Red CMXRos	C1035	Beyotime Biotechnology, China
Penicillin-Streptomycin-Amphotericin B	C0224	Beyotime Biotechnology, China
Cell Mitochondrial Isolation Kit	C3601	Beyotime Biotechnology, China
Enhanced ATP Assay Kit	S0027	Beyotime Biotechnology, China
Quick-block™	P0252	Beyotime Biotechnology, China
CCK-8	40203ES	Yeasen Biotechnology, China
MitoSOX	40778ES	Yeasen Biotechnology, China
PI	BS147	Biosharp, China
Seahorse XFe24 FluxPak mini	102342–100	Agilent, USA
Seahorse Cell Mito Stress Test kit	103015–100	Agilent, USA
XF DMEM Medium	103575–100	Agilent, USA
XF 1.0 M Glucose Solution	103577–100	Agilent, USA
XF 100 mM Pyruvate Solution	103578–100	Agilent, USA
XF 200 mM Glutamine Solution	103579–100	Agilent, USA
Mitochondrial complex I/NADH-CoQ reductase Activity Assay Kit	BC0515	Solarbio, China
TRIzol	15596026CN	Thermo Fisher Scientific, USA
Prime Script™ RT	RR420Q	TaKaRa, Japan
Mitochondrial DNA Extraction Kit	D2021	Saint-bio, China

Table 2
Antibodies and dilutions used for immunoblot analysis.

Antibody	Dilution	Reference, Company
anti-GLAST	1:1000	20785-1-AP, Proteintech Biotechnology
anti-GLT-1	1:1000	22515-1-AP, Proteintech Biotechnology
anti-GS	1:1000	80636, Cell Signaling Technology
anti-GFAP	1:1000	AF1177, Beyotime Biotechnology
anti-DRP1	1:1000	12957-1-AP, Proteintech Biotechnology
anti-OPA1	1:1000	27733-1-AP, Proteintech Biotechnology
anti-MFN2	1:1000	12186-1-AP, Proteintech Biotechnology
anti-phospho Drp1 (ser616)	1:1000	3455, Cell Signaling Technology
anti-H_1R	1:500	861759, Zenbio
anti-H_2R	1:500	861760, Zenbio
anti-H_3R	1:1000	ab96787, Abcam
anti-COXIV	1:1000	11242-1-AP, Proteintech Biotechnology
anti-β-tubulin	1:1000	30302ES60, Yeasen Biotechnology
Goat Anti-Rabbit IgG	1:4000	7074, Cell Signaling Technology

Table 3
Antibodies and dilutions used for immunofluorescence analysis.

Antibody	Dilution	Reference, Company
anti-H_1R	1:400	AHR-001, Alomone Labs
anti-H_2R	1:400	AHR-002, Alomone Labs
anti-H_3R	1:400	DF4981, Affinity Biosciences LTD
anti-GFAP	1:50	sc-65343, Santa Cruz Biotechnology
Goat Anti-Rabbit IgG Fluor594	1:250	S0006, Affinity Biosciences LTD
Goat Anti-Mouse IgG Fluor488	1:250	S0017, Affinity Biosciences LTD

2.3. Animal studies

Mice were randomly divided into four groups of fifteen mice each: normal control group (NC group), glucose variability group (GV group), normal control + histidine group (NC + his group) and glucose variability + histidine group (GV + his group), and the experimental protocol was based on previous studies (Fig. 1**A**) [8]. Specifically, mice in the GV and GV + his groups were subjected to a single intraperitoneal injection of 150 mg/kg streptozotocin (STZ) to establish a T1D model. When random blood glucose levels exceeded 16.7 mM and successful induction of diabetic status was confirmed, insulin replacement therapy was started with an initial dose of 2 IU/kg body weight per day, administered subcutaneously, and subsequently adjusted according to blood glucose levels. The aim of this treatment was to control blood glucose levels, avoid extreme hyperglycemia, maintain a stable glycemic baseline, and ensure that experimental animals maintained healthy and normal weight gain during long-term experiments. During insulin treatment, recurrent non-severe hypoglycemic states were induced by administering insulin and glucose twice a week for 2 h each time, over a period of 4 weeks, to induce increased glucose variability. In hypoglycemia experiments, the initial dose of regular insulin was 4.0mIU/g, and the dose was adjusted every 30 min according to blood glucose levels to keep blood glucose in the range of 2.0–3.0 mmol/l for two hours. The hypoglycemic state was terminated by intragastric administration of glucose (1 mg/kg). During this period, no seizures or coma were observed. All non-diabetic mice received the same volume of saline injection. Mice in the GV + his and NC + his groups received 1 g/kg L-histidine intraperitoneally 30 min before each hypoglycemia induction, while the other groups received an equal volume of saline. Body weight and random blood glucose levels were measured regularly weekly in all mice during the experiment (Fig. 1**C-D**).

2.4. Immunofluorescence

Mouse right brain hemispheres were fixed in 4 % formaldehyde, embedded in paraffin, and sectioned into 5-μm-thick coronal slices. Sections were deparaffinized, dehydrated, and underwent antigen retrieval before blocking with 1 % BSA. They were incubated with primary antibodies overnight at 4 °C, followed by fluorescein-conjugated secondary antibodies for 2 h at room temperature, and stained with DAPI for nuclear visualization. The prepared sections were then examined under a fluorescence microscope. The colocalization ratio is obtained by calculating Manders' Colocalization Coefficients (MCC) through Coloc 2, a plug-in of Image J software. For further details on the methodology and the specific steps involved in calculating MCC, please refer to the Coloc 2 plugin documentation available at https://imagej.net/plugins/coloc-2.

2.5. Targeting energy metabolomics

Approximately 50 mg of hippocampal tissue was homogenized in 500 μL of 70 % methanol at −20 °C, vortexed for 3 min, and centrifuged at 12000 rpm for 10 min at 4 °C, from which 300 μL of supernatant was collected. This was further centrifuged under similar conditions after which 200 μL of the final supernatant was prepared for analysis using Shimadzu LC Nexera X2 UHPLC coupled with a QTRAP 5500 LC-MS/MS (AB Sciex). Chromatographic separation was performed with ACQUITY UPLC UPLC BEH Amide analytic column. The mobile phase was performed in buffer A (10 mM ammonium acetate in water, pH 8.8) and buffer B (10 mM ammo-nium acetate in acetonitrile/water (95/5), pH 8.2). The gradient elution was 95–61 % buffer B in 7 min, 61–44 % buffer B at 9 min, 61–27 % buffer B at 9.2 min, and 27–95 % buffer B at 10 min. The column was equilibrated with 95 % buffer B at the end. 13C-nicotinic acid (Toronto Research Chemicals) was added as the inter-nal standard. MultiQuant 3.0.2 software (AB Sciex) was used to integrate the extracted MRM peaks. All those metobolites were detected by MetWare (https://www.metware.cn/) based on the AB Sciex QTRAP 6500 LC-MS/MS platform. Unsupervised PCA (principal component analysis) was performed by statistics function prcomp within R (https://www.r-project.org). The data was unit variance scaled before unsupervised PCA.

2.6. Cell culture and treatment

Establish a primary mouse astrocyte culture model with alternating high and low glucose conditions to simulate high GV, as previously (Fig. 1**B**) [16,19]. Specifically, cerebral cortex was extracted from the skull of C57BL/6 suckling mice within 24 h of birth. First, the cortical tissue was carefully dissected from the meninges, then the tissue was cut into small pieces and digested using 0.25 % trypsin for 15 min. The tissue was then gently transferred to a filter to collect the isolated cells. Cells were planted in Dulbecco's Modified Eagle Medium (DMEM) containing 10 % fetal bovine serum (FBS) at 37 °C in humidified 5 % CO_2/95 % air and the medium was changed every 3 days. When cell confluency reached 80–85 %, microglia were removed by overnight shaking on a shaker and new medium was replaced the following day.

Table 4
Primers sequences used in the current study.

Gene	Forward primer sequence (5′-3′)	Reverse primer sequence (5′-3′)
COXI	TCCAACTCATCCCTTGACATCG	CCCAGGAAATGTTGAGGGAAGA
ND1	CTAGCAGAAACAAACCGGGC	CCGGCTGCGTATTCTACGTT
H_3R	TGCTGTATGGGCCTGCCATCC TGAGTTGG	CACCATCTTCATGCGCTTCTCCAGGGATGC
GAPDH	TTCCCGTTCAGCTCTGGG	CCCTGCATCCACTGGTGC

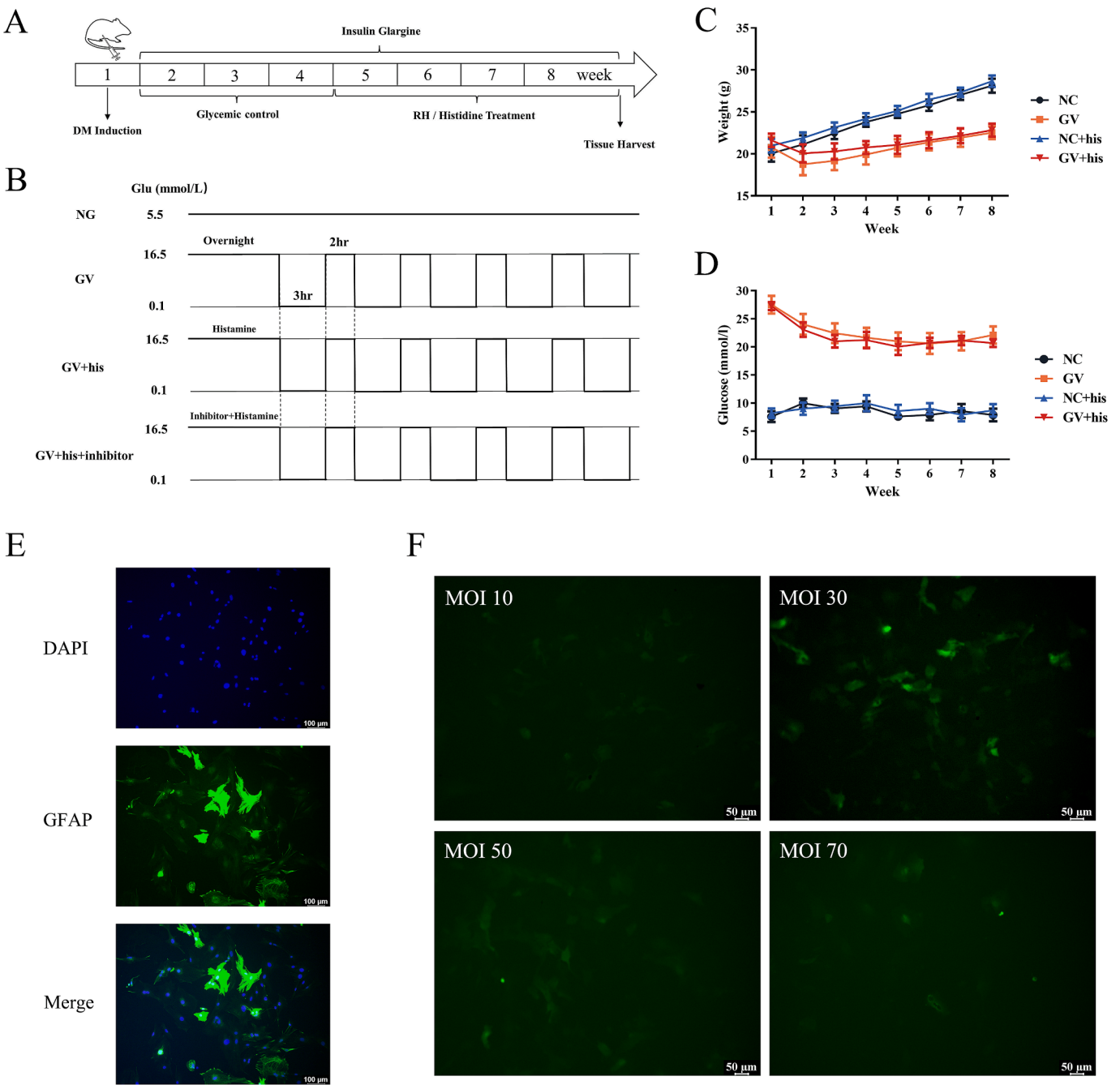

Fig. 1. Animal and cell model interventions: construction, validation, and multiplicity of lentiviral infection. (A) Schematic diagram of animal model construction. (B) Schematic representation of in vitro cell model intervention. (C) Body weight of mice. (D) Random blood glucose of mice. N = 15. (E) Astrocyte identification. Scale bar = 100 μm. (F) Determination of the multiplicity of infection (MOI) of lentivirus. Scale bar = 50 μm. DM, diabetes mellitus; RH, recurrent hypoglycemia; DAPI, 4′,6-diamidino-2-phenylindole; GFAP, glial fibrillary acidic protein; MOI, multiplicity of infection; NC, normal control; NG, normal glucose (5.5 mM); GV, glucose variability; NC + his, normal control + histidine; GV + his, glucose variability + histidine/histamine; GV + his + inhibitor, glucose variability + histidine/histamine + histamine receptor inhibitor.

When astrocyte density reached 95 %, passages were performed for subsequent experiments. All experiments were performed when cell confluency reached 80–85 %. To identify astrocytes, cells were first fixed using 4 % paraformaldehyde and subsequently treated with 0.1 % Triton-X-100 for 15 min to permeate the cell membrane. Following this, cells were incubated overnight at 4 °C with monoclonal rabbit antibody against GFAP. Cells were then washed three times with PBS and then incubated with Alexa Fluor 488-conjugated goat anti-rabbit IgG (H + L) for 1 h at room temperature. Finally, nuclei were stained by treatment with DAPI staining solution for 5 min at room temperature and immunofluorescence images were acquired using a fluorescence microscope (Fig. 1**E**).

Specific procedures of establishing the high glucose variability model in vitro were as follows: first, astrocytes were cultured overnight in DMEM medium containing 16.5 mmol/L glucose, and astrocytes cultured in DMEM containing 5.5 mmol/L glucose served as the control group. Astrocytes in the relevant intervention groups will be first incubated for half an hour with inhibitors of histamine receptor subtypes at concentrations of the H_1R inhibitor pyrilamine (10 μM), the H_2R inhibitor cimetidine (1 μM), and the H_3R inhibitor thioperamide (1 μM)

[20,21]. Following this, the original medium was removed and replaced with a new medium containing 1 mM histamine and incubation continued for 17 h. When performing recurrent low glucose experiments, the original medium was first aspirated and washed for 30 min using PBS with the aim of depleting intracellular glucose. Then, the medium was changed to isosmolality low-glucose medium (DMEM containing 0.1 mmol/L glucose) and incubated for 3 h, after which the medium was changed back to the original medium and incubated for 2 h. This process was performed five consecutive times. In order to eliminate the possible effects brought about by differences in osmolality, D-mannitol was supplemented at 5.4 mM and 16.4 mM in the medium with 5.5 mmol/L and 16.5 mmol/L glucose, respectively, to ensure the accuracy of the experiment.

2.7. Gene overexpression experiments

H_3R cDNA was cloned into GV492-Green Fluorescent Protein (GFP) vector. GV492-H_3R vector and control vector were packaged into lentiviral transfection system and purchased from Shanghai Genechem Co., Ltd. (Shanghai, China). Primary astrocytes were infected with lentiviruses overexpressing H_3R at a multiplicity of infection (MOI) of 30 (Fig. 1**F**). GFP unloaded lentivirus-infected astrocytes served as negative controls.

2.8. Cell viability and apoptosis assay

To assess the cell viability of astrocytes, we performed assays using the CCK-8 kit. 10 μL CCK-8 reagent was added to each well and incubated for 1 h. Optical density (OD) values were measured for each well using a microplate reader at 450 nm. To detect apoptosis in astrocytes, we stained using Hoechst 33,342 and PI staining solution. Cells were stained with Hoechst 33,342 and PI for 30 min at 4 °C in the dark according to the kit 's instructions.

2.9. Cell glutamate reuptake capacity and glucose uptake assay

Glutamate uptake capacity was determined using a glutamate assay kit. After washing the cells three times with Hank 's balanced salt solution (HBSS), 400 μL HBSS containing 200 μM glutamate was added to each well and incubated for 3 h, and the supernatants were collected. Subsequently, 100 μL of the reaction mixture was added to each well and the OD value of each well was measured with a microplate reader at 450 nm wavelength. Glutamate reuptake content was calculated as the amount of glutamate initially added to the medium (200 μM) minus the glutamate content detected by the kit and finally normalized to the protein content in the corresponding cells.

Glucose uptake capacity is based on the glucose uptake test kit. Specifically, after completion of the intervention in each group, cells were incubated for 20 min after addition of 10 mM 2-DG (deoxyglucose). Subsequently, reaction mixture was added to each well and the OD value of each well was measured with a microplate reader at 412 nm wavelength and finally normalized to the protein content in the corresponding cells.

2.10. Mitochondrial isolation

After different treatments, astrocytes were obtained and then manipulated according to the instructions of the cell mitochondria isolation kit. Briefly, cells were resuspended in mitochondrial extraction reagent (provided in the kit) and homogenized with a micro-homogenizer and then placed in an ice bath for 15 min. The homogenate was centrifuged at 600 × g for 10 min at 4 °C. Supernatants were collected and centrifuged at 11000 × g for 10 min at 4 °C. Finally, mitochondrial fractions were collected from the precipitates for subsequent experiments. Mitochondria were isolated for subsequent immunoblotting assays of phosphor-dynamin-related protein 1 (DRP1) at ser616 and COXIV proteins.

2.11. Mitochondrial morphometry

Mitochondrial morphology was assessed by MitoTracker Red staining under confocal laser scanning microscopy. Cells were incubated with 250 nM MitoTracker Red for 30 min at 37 °C in the dark. Subsequently, cells were washed with PBS and pre-warmed fresh medium was added. Mitochondrial morphology was observed using confocal laser scanning microscopy with MitoTacker Red excitation at 579 nm. Mitochondria were labeled with red fluorescence. Mitochondrial aspect ratio and form factor parameters reflecting individual mitochondrial morphology were calculated using ImageJ software (RRID: SCR_003070).

2.12. Mitochondrial ROS test

Mitochondrial ROS levels were measured by MitoSOX staining. Cells were washed three times with PBS buffer. Subsequently, cells were incubated with 5 μM MitoSOX for 30 min at 37 °C in the dark. Cells were then washed three times and mitochondrial ROS were visualized under a fluorescence microscope. Fluorescence intensity was calculated using ImageJ software.

2.13. ATP content test

ATP content was determined using an enhanced cellular ATP assay kit according to the kit's instructions. Cells were homogenized and lysates were centrifuged at 12,000×*g* for 5 min at 4 °C. The supernatant was added to a 96-well plate and mixed. Luminescence signals were collected with a luminometer. Total ATP levels were calculated using a standard curve and then normalized using protein concentration.

2.14. Mitochondrial complex I activity test

Complex I activity was assessed using the Mitochondrial Respiratory Chain Complex I Enzyme Activity Microplate Assay Kit according to the kit's instructions. Briefly, cells were harvested and lysed on ice for 30 min. After centrifugation at 16,000×*g* for 20 min at 4 °C, supernatants were collected. Subsequently, 200 μL of sample was added to the 96-well reaction plate included in the kit and incubated for 3 h at room temperature. Following washing with wash buffer, 200 μL of test solution was added and OD values were determined for the indicated times in kinetic mode.

2.15. Mitochondrial oxygen consumption rate (OCR)

Mitochondrial OCR was assessed by a mitochondrial pressure test kit using a Seahorse Extracellular Flux (Seahorse XFe24) analyzer. Oligomycin, carbonyl cyanide phosphor-(p)-trifluoromethoxy phenylhydrazone (FCCP), and rotenone/antimycin A (Rotenone + Antimycin A) were diluted in XFe24 assay medium (pH = 7.40) and added to subsequent extraction columns to reach final concentrations of 1, 2, 0.5, and 0.5 μM, respectively. Oligomycin, FCCP, and Rotenone + Antimycin A were injected sequentially into each well. OCR was recorded and calibrated based on the number of cells per well. Samples with negative OCR values were excluded from analysis.

2.16. RT-qPCR

Total RNA and DNA were extracted from astrocytes using TRIzol reagent and a mitochondrial DNA extraction kit, respectively. RNA was reverse transcribed with the Prime Script™ RT kit, and H_3R mRNA levels were quantified by RT-qPCR using SYBR® Premix Ex Taq™ II, with GAPDH as the normalization control. Expression was calculated using the comparative cycle threshold (Ct) method (ΔΔCt). Similar procedures were followed for mitochondrial DNA analysis.

2.17. Immunoblot analysis

Proteins extracted using lysates containing protease and phosphatase inhibitors. Proteins (20 μg) were separated by sodium dodecyl sulfate–polyacrylamide gel and transferred to polyvinylidene difluoride membranes. After blocking with blocking buffer for 30 min, membranes were incubated with primary antibodies overnight at 4 °C. Membranes were washed three times with Tris-HCl buffered saline solution and incubated with horseradish peroxidase-conjugated secondary antibodies for 2 h at 37 °C. Band densities were analyzed using ImageJ software (RRID: SCR_003070) and normalized to β-tubulin or COXIV levels.

2.18. Statistical analysis

All experiments were performed at least three times. Data were presented as mean ± standard error (Mean ± SEM) using one-way analysis of variance (ANOVA) with Tukey 's test as the subsequent multiple comparison method. All mapping and statistical analyses were performed using GraphPad Prism software version 9.0.0 (RRID: SCR_002798). P values less than 0.05 were considered statistically significant.

3. Results

3.1. The impact of histidine intervention on HR and glutamate metabolic clearance function in hippocampal astrocytes of GV mice

We conducted immunofluorescence co-localization experiments using glial fibrillary acidic protein (GFAP) and HR subtypes to explore HR system changes in astrocytes under increased GV. The results indicated decreased expression levels of H_1R, H_2R, and H_3R in the GV group compared to the NC group, with significant increases in H_1R and H_3R following histidine intervention (Fig. 2**A-C**). Further immunoblot analysis of hippocampal proteins related to glutamate metabolic clearance revealed a notable decrease in the expression of glutamate-aspartate transporter (GLAST), glutamate transporter-1 (GLT-1), and glutamate synthetase (GS) in the GV group, contrasted with an increase in GFAP expression. Post-histidine intervention, there was a significant recovery in the expression of GLAST, GLT-1, and GS, and a decrease in GFAP expression (Fig. 2**D-H**). These findings suggest that histidine intervention may contribute to reducing the risk of neurotoxicity in conditions of increased glucose variability by potentially enhancing glutamate transporter expression in astrocytes, corroborating our observations on HR expression changes and underscoring the potential role of HR system alterations in modulating astrocyte function in the hippocampus.

3.2. The impact of histidine intervention on the energy metabolism pattern of hippocampal tissue in GV mice

We utilized energy metabolomics to study the energy metabolism patterns in the hippocampus of model mice with increased GV following histidine intervention, aiming to establish the mechanistic clues of the astrocyte HR system in regulating glutamate metabolic clearance. Principal component analysis revealed significant metabolic profile differences between the NC, GV, and GV + his groups along principal component 1 (PC1, 54.22 % variance), with less distinction between NC and NC + his groups. Metabolite analysis indicated that glycolysis was disrupted under increased GV, with key glycolytic metabolites like glucose, fructose 1,6-diphosphate, dihydroxyacetone phosphate

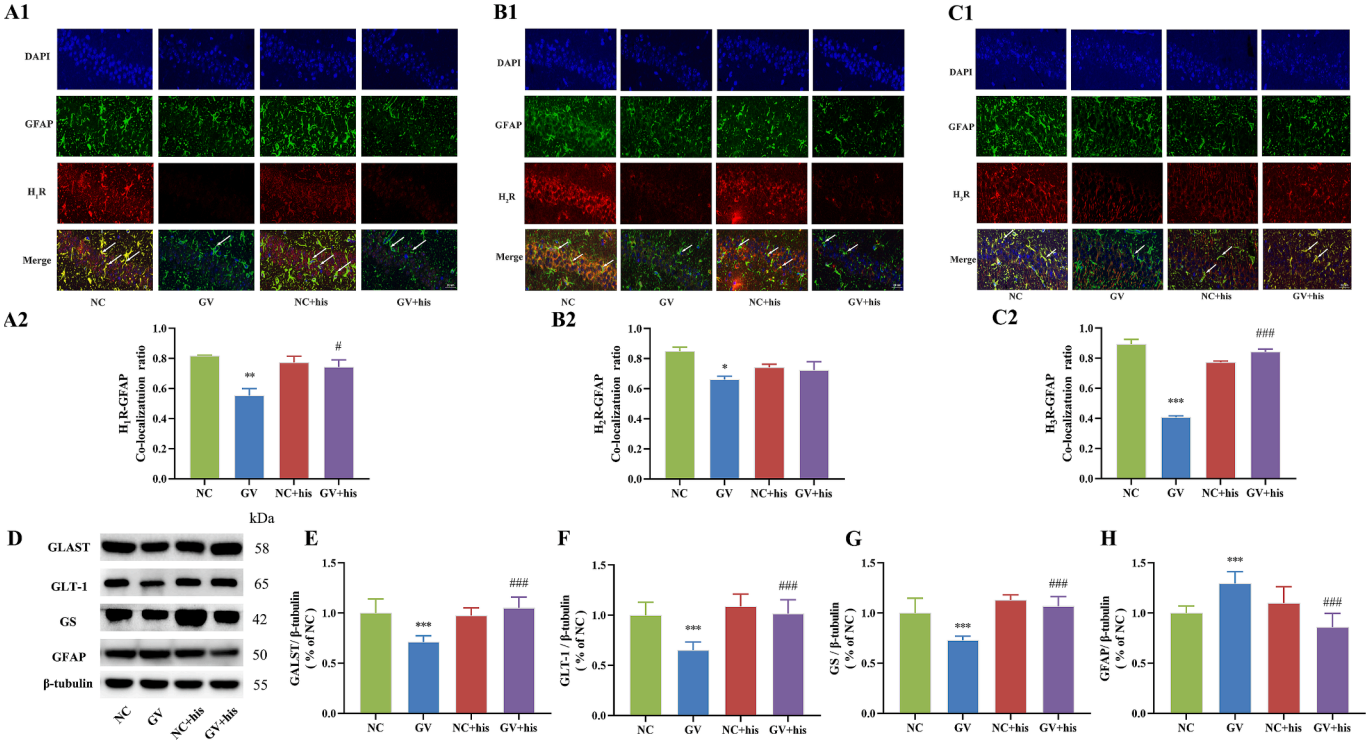

Fig. 2. The impact of histidine intervention on HR and glutamate metabolic clearance function in hippocampal astrocytes of GV mice. (A1-C1) Representative images of immunofluorescence co-localization of H_1R, H_2R and H_3R in the CA1 region of the hippocampus, respectively; Scale bar: 20 μm. Arrows show colocalized astrocytes in hippocampal CA1. (A2-C2) Semi-quantitative results of GFAP co-localization with H_1R, H_2R, and H_3R, respectively. N = 3. * $P < 0.05$, ** $P < 0.01$, *** $P < 0.001$, GV vs. NC; # $P < 0.05$, ### $P < 0.001$, GV + his vs. GV. (D) Representative immunoblot images of proteins associated with glutamate metabolic clearance. (E-H) Relative protein levels of GLAST, GLT-1, GS and GFAP. N = 6. *** $P < 0.001$, GV vs. NC; ### $P < 0.001$, GV + his vs. GV. DAPI, 4′,6-diamidino-2-phenylindole; GLAST, glutamate-aspartate transporter; GLT-1, glutamate transporter-1; GS, glutamine synthetase; GFAP, glial fibrillary acidic protein; H_1R, histamine receptor 1; H_2R, histamine receptor 2; H_3R, histamine receptor 3; NC, normal control; GV, glucose variability; NC + his, normal control + histidine; GV + his, glucose variability + histidine.

(DHAP), and others reduced, while Glucose-6-P and lactate levels were elevated. Post-histidine intervention, levels of glucose, Glucose-6-P, DHAP, glyceraldehyde 3-phosphate, and lactate significantly increased (Fig. 3**A-H**). Abnormalities were also noted in the tricarboxylic acid (TCA) cycle, with increased levels of citrate, isocitrate, fumarate, and malate in the GV group, but decreased acetyl-CoA and succinate (Fig. 3**I-N**). Oxidative phosphorylation was impacted as well, with reduced levels of NAD+, cAMP, ATP, and ADP (Fig. 3**Q-T**). Histidine intervention did not significantly alter most of these metabolites. Additionally, while glutamate and L-glutamine levels were initially unchanged between GV and NC groups, both increased following histidine intervention (Fig. 3**O-P**). Notably, alanine levels increased in the GV group compared to the NC group, but remained unchanged following histidine intervention (Fig. 3**U**). Due to the distinct regulatory mechanisms of phosphofructokinase and the expression of pyruvate carboxylase variants in neurons and astrocytes, the observed metabolic changes may be specific to astrocytes. Further research on the impact of increased GV on astrocytic mitochondrial metabolism will enhance our understanding of HRs in neuroprotection.

3.3. Activation of HRs enhanced glutamate reuptake by astrocytes in the context of high GV

To investigate the effect of increased GV on specific brain cell injury, we developed a primary astrocyte culture model and simulated increased GV in vivo by alternating high and low glucose culture conditions. Our results showed decreased viability and increased apoptosis in astrocytes in the GV group compared to the NG group. Histamine intervention improved cell viability and reduced apoptosis (Fig. 4**A-C**). We also observed decreased expression of H_1R, H_2R, and H_3R in the GV group, which increased after histamine intervention, confirming HR activation in astrocytes (Fig. 4**D-G**). Further, we examined whether HR activation enhances the expression of glutamate metabolism-related proteins. In the GV group, there was a significant decrease in GLAST, GLT-1, and GS protein levels, and an increase in GFAP expression, which reversed following histamine intervention (Fig. 4**H-L**). Additionally, glutamate reuptake capacity was significantly lower in the GV group but improved after histamine treatment; this improvement was reversed by inhibiting HR subtypes (Fig. 4**M-N**). These findings suggest that HR activation in astrocytes not only boosts cell viability and decreases apoptosis but also promotes the expression of proteins involved in glutamate clearance, enhancing glutamate reuptake and potentially offering neuroprotection against brain injury caused by increased GV. We also assessed glucose uptake and lactate secretion in astrocytes under different conditions. Both were significantly elevated in the GV group compared to the NG group, with no significant changes post-histamine intervention (Fig. 4**O-P**).

3.4. HRs regulated mitochondrial function of astrocytes in the context of high GV

Previous studies have shown that alleviating mitochondrial dysfunction can restore astrocyte function in environments of increased GV [16,19]. We further explored mitochondrial function in astrocytes using histamine and specific inhibitors for each receptor subtype. Using MitoSOX staining, we found that mitochondrial ROS levels were

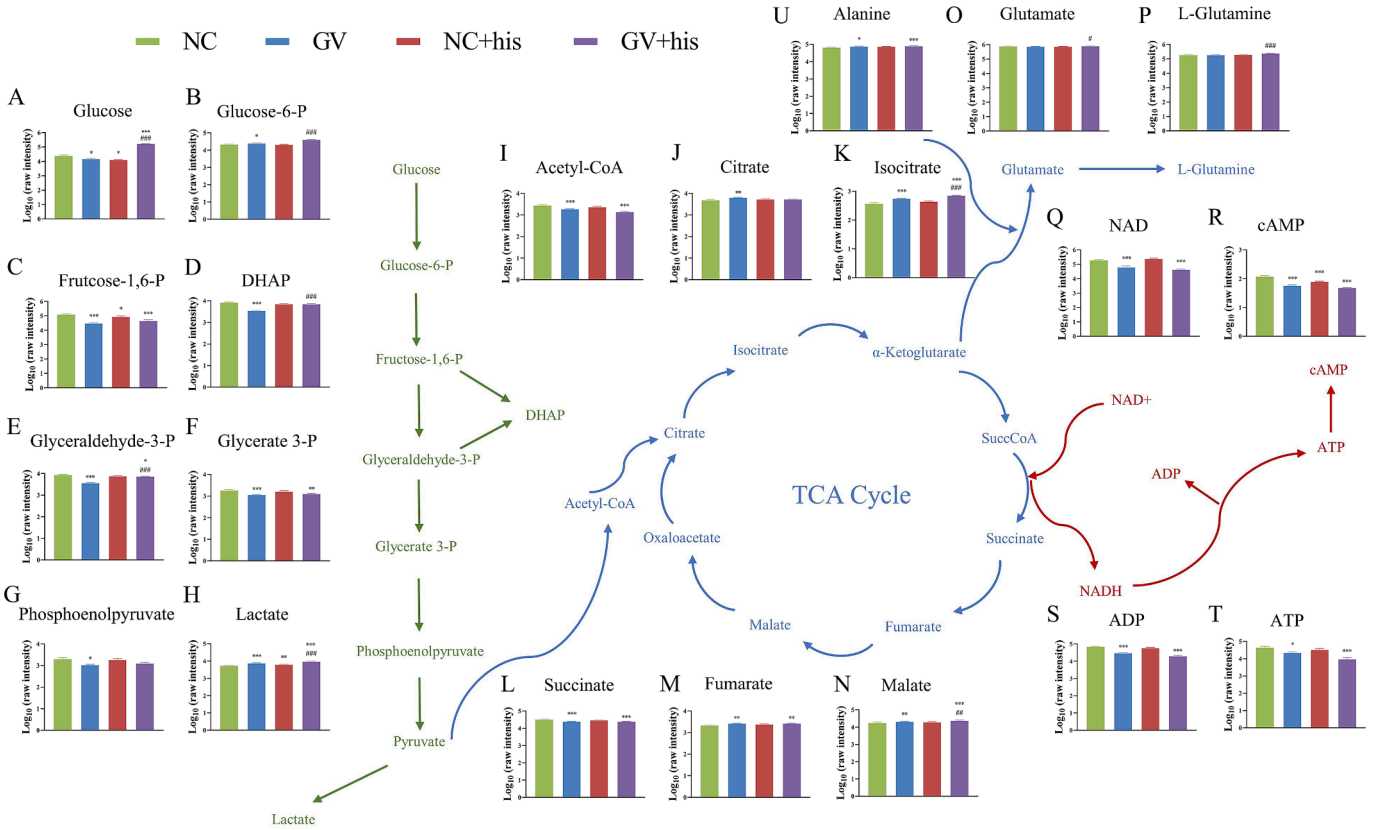

Fig. 3. The impact of histidine intervention on the energy metabolism pattern of hippocampal tissue in GV mice. (A-H) Quantitative analysis of glycolytic pathway-related metabolites. (I-P) Quantitative analysis of metabolites involved in TCA cycle and glutamate metabolism pathway. (Q-T) Quantitative analysis of metabolites associated with oxidative phosphorylation metabolic pathways. (U) Quantitative analysis of alanine metabolites. Data were log transformed (log10). N = 6. * $P < 0.05$, ** $P < 0.01$, *** $P < 0.001$, vs. NC; # $P < 0.05$, ## $P < 0.01$, ### $P < 0.001$, GV + his vs. GV. DHAP, dihydroxyacetone phosphate; NAD, nicotinamide adenine dinucleotide; cAMP, cyclic adenosine monophosphate; ADP, adenosine diphosphate; ATP, adenosine triphosphate; NC, normal control; GV, glucose variability; NC + his, normal control + histidine; GV + his, glucose variability + histidine.

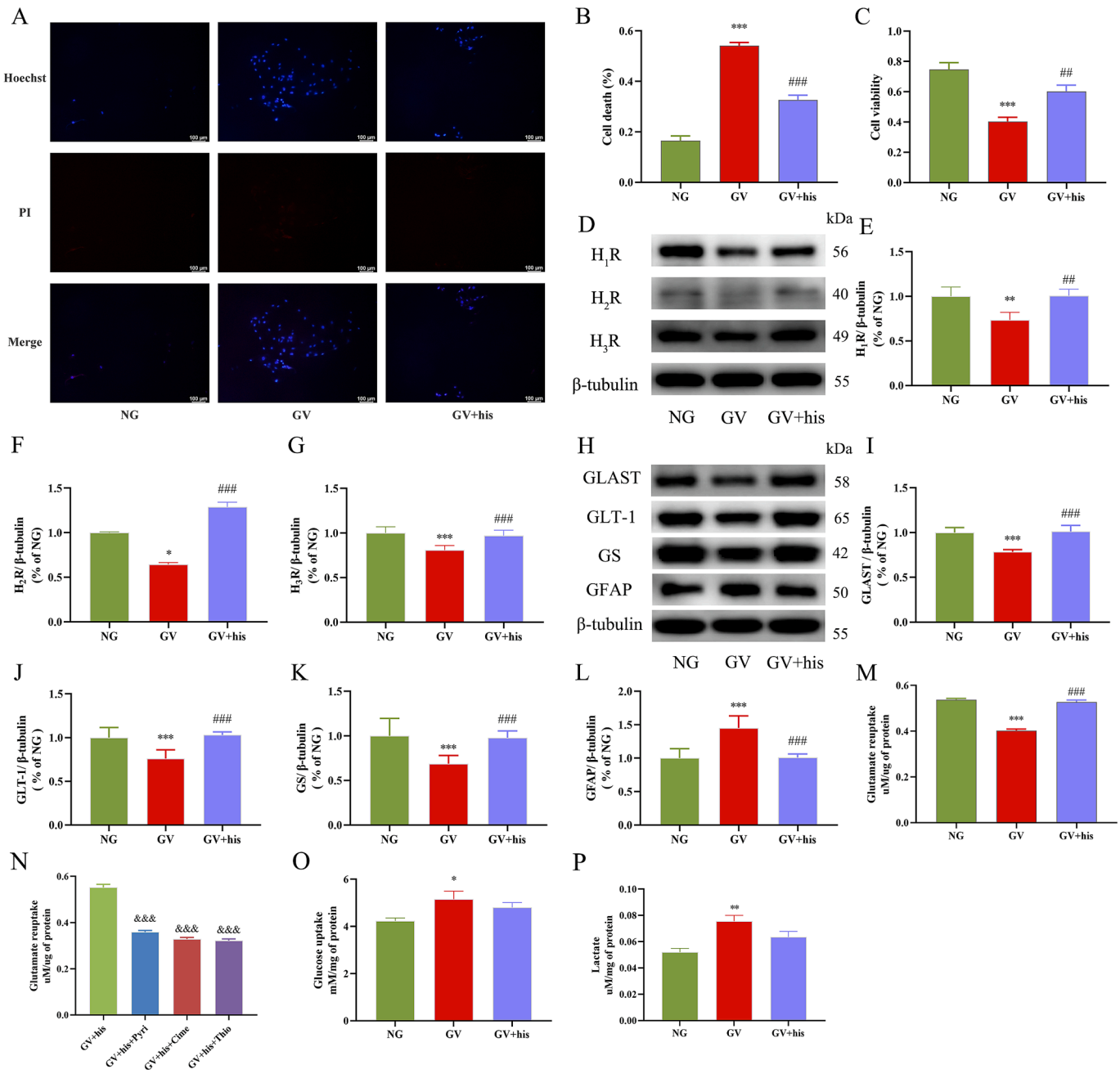

Fig. 4. Activation of HRs enhanced glutamate reuptake by astrocytes in the context of high GV. (A) Schematic representation of astrocyte apoptosis staining. (B) Percentage of cell death. N = 3. (C) Cell viability. N = 6. (D) Representative immunoblot images of HR proteins. (E-G) Relative protein levels of H_1R, H_2R and H_3R. N = 6. (H) Representative immunoblot images of proteins associated with glutamate metabolic clearance. (I-L) Relative protein levels of GLAST, GLT-1, GS and GFAP. N = 6. (M–N) Glutamate reuptake capacity. N = 6. (O-P) Capacity of glucose uptake and lactate secretion. N = 5. * $P < 0.05$, ** $P < 0.01$, *** $P < 0.001$, GV vs. NG; ## $P < 0.01$, ### $P < 0.001$, GV + his vs. GV; &&& $P < 0.001$, vs. GV + his. PI, propidium iodide; GLAST, glutamate-aspartate transporter; GLT-1, glutamate transporter-1; GS, glutamine synthetase; GFAP, glial fibrillary acidic protein; H_1R, histamine receptor 1; H_2R, histamine receptor 2; H_3R, histamine receptor 3; NG, normal glucose (5.5 mM); GV, glucose variability; GV + his, glucose variability + histamine; GV + his + Pyri, glucose variability + histamine + histamine receptor 1 inhibitor; GV + his + Cime, glucose variability + histamine + histamine receptor 2 inhibitor; GV + his + Thio, glucose variability + histamine + histamine receptor 3 inhibitor.

significantly higher in astrocytes with inhibited H_1R, H_2R, and H_3R compared to the GV + histamine group (Fig. 5**A-B**). Additionally, mitochondrial DNA (mtDNA) replication levels were significantly reduced upon HR inhibition (Fig. 5**C**), aligning with increased mitochondrial ROS, which can damage mtDNA and affect its replication [22]. Given that mtDNA encodes key proteins for the electron transport chain, disruptions in mtDNA replication can impair mitochondrial respiratory function [22]. We assessed mitochondrial respiratory capacity using a Seahorse XF24 analyzer, observing a decline in various respiratory parameters upon HR inhibition, particularly after H_3R inhibition (Fig. 5**D-I**). Further analyses of cellular ATP content and mitochondrial respiratory chain complex I activity confirmed these findings (Fig. 5**J-K**). These results highlight the critical role of histamine and its receptors, especially H_3R, in maintaining mitochondrial function and supporting respiratory activity and ATP production in astrocytes under increased GV conditions.

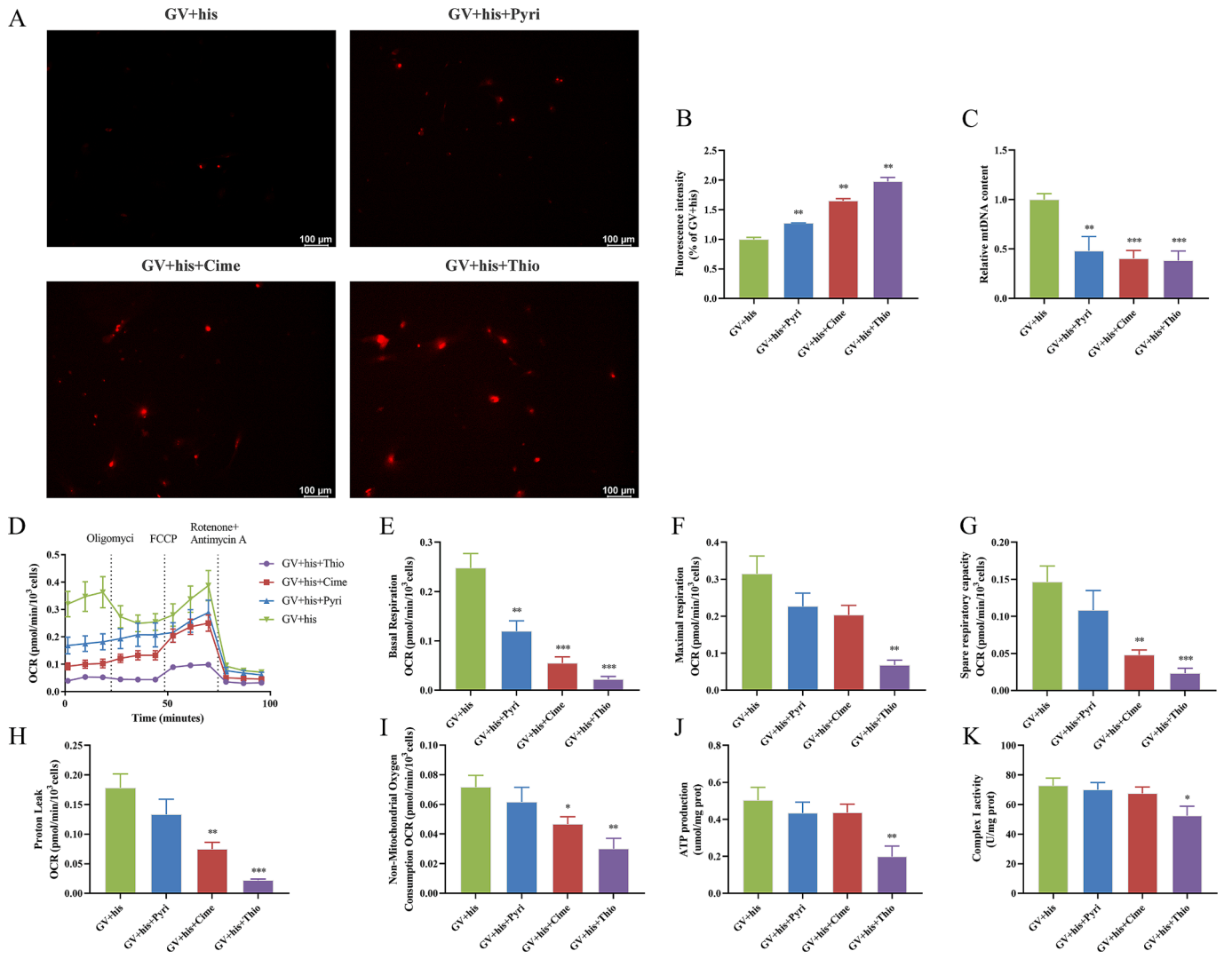

Fig. 5. HRs regulated mitochondrial function of astrocytes in the context of high GV. (A-B) Mitochondrial ROS levels. N = 3. Scale bar: 100 μm. (C) Copy number of mtDNA. N = 6. (D) Real-time OCR. (E) Basal respiratory OCR. (F) Maximal respiration OCR. (G) Spare respiratory capacity OCR. (H) Proton leak OCR. (I) Non-mitochondrial OCR. N = 5–6. (J) ATP production. N = 6. (K) Mitochondrial respiratory chain complex I activity. N = 6. * $P < 0.05$, ** $P < 0.01$, *** $P < 0.001$, vs. GV + his. FCCP, carbonyl cyanide 4-(trifluoromethoxy) phenylhydrazone; ROS, reactive oxygen species; OCR, oxygen consumption rate; GV + his, glucose variability + histamine; GV + his + Pyri, glucose variability + histamine + histamine receptor 1 inhibitor; GV + his + Cime, glucose variability + histamine + histamine receptor 2 inhibitor; GV + his + Thio, glucose variability + histamine + histamine receptor 3 inhibitor.

3.5. HRs regulated mitochondrial dynamics of astrocytes in the context of high GV

Mitochondrial fission and fusion (dynamics) homeostasis is the premise and basis for maintaining mitochondrial number, morphology and function [23]. Previous studies have shown that recurrent hypoglycemia-induced increases in GV lead to excessive mitochondrial fission in mouse hippocampal tissue, disrupting mitochondrial homeostasis and causing cognitive decline [7]. We explored how histamine and its receptors regulate mitochondrial function in astrocytes under increased GV conditions. Using MitoTracker Red and confocal microscopy, we observed mitochondrial morphology in astrocytes and analyzed aspect ratio and form factor. Both parameters decreased, particularly with H_3R inhibition, indicating increased mitochondrial fragmentation (Fig. 6**A–C**). We also examined proteins regulating mitochondrial dynamics. Post-HR inhibition, especially H_3R, there was an increase in total and phosphorylated DRP1 at Ser616, and a decrease in mitofusin-2 (MFN2) and optical atrophy 1 (OPA1) expression, suggesting that H_3R inhibition affects mitochondrial morphology and function by altering proteins involved in mitochondrial fission and fusion (Fig. 6**D-H**).

3.6. H_3R balanced mitochondrial dynamics to restore the glutamate reuptake function of astrocytes in the context of high GV

We investigated the role of H_3R in astrocyte glutamate metabolic clearance by overexpressing H_3R in astrocytes and administering a mitochondrial fusion inhibitor (MFI8, 20 μM, 6 h) [24]. Overexpression of H_3R significantly increased both protein and mRNA levels of H_3R, confirming successful transfection (Fig. 7**A-C**). Additionally, H_3R overexpression upregulated the protein expression of glutamate transporters GLAST and GLT-1, and the metabolic enzyme GS, enhancing glutamate reuptake capacity. However, these effects were diminished by MFI8, which reduced the levels of GLAST, GLT-1, and GS (Fig. 7**D-H**). These findings indicate that H_3R can improve glutamate clearance in astrocytes in high GV environments through mechanisms linked to mitochondrial dynamics.

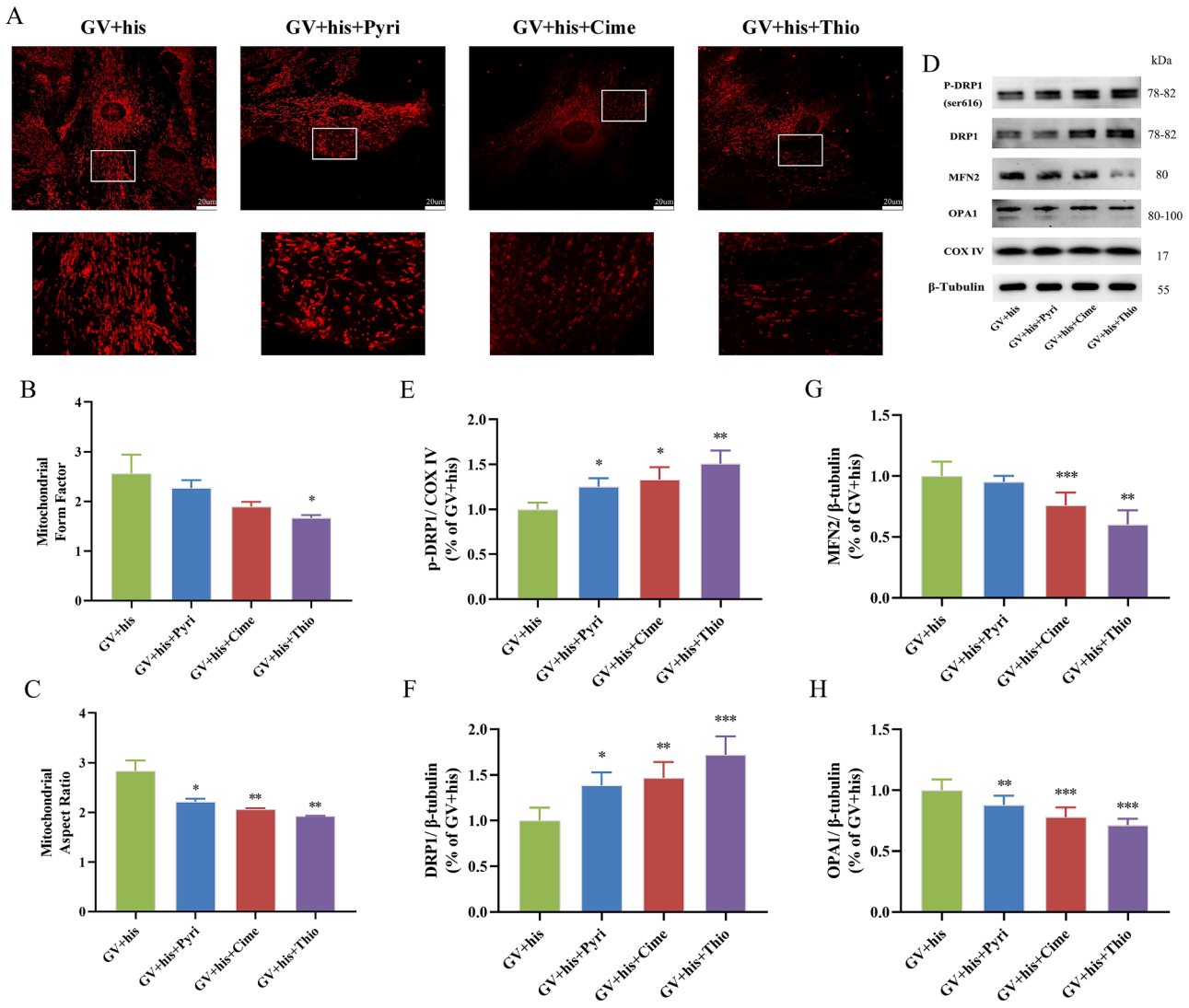

Fig. 6. HRs regulated mitochondrial dynamics of astrocytes in the context of high GV. (A) Complete and partially magnified images of the mitochondrial network. Scale bar: 20 μm. (B-C) mitochondrial aspect ratio and form factor. N = 3. (D) Representative immunoblot images of proteins associated with mitochondrial dynamics. (E-H) Relative protein levels of P-DRP1 (ser616), DRP1, MFN2 and OPA1. N = 6. * P < 0.05, ** P < 0.01, *** P < 0.001, vs. GV + his. DRP1, dynamin-related protein 1; MFN2, mitofusin 2; OPA1, optic atrophy 1; GV + his, glucose variability + histamine; GV + his + Pyri, glucose variability + histamine + histamine receptor 1 inhibitor; GV + his + Cime, glucose variability + histamine + histamine receptor 2 inhibitor; GV + his + Thio, glucose variability + histamine + histamine receptor 3 inhibitor.

4. Discussion

In this study, we investigated the mechanisms by which histamine and its receptor system preserve glutamate metabolic clearance capacity through the regulation of mitochondrial function in astrocytes under conditions of recurrent hypoglycemia-induced increased GV. Our findings unveil the key role of H_3R in this process, along with elucidating the underlying mechanism involving mitochondrial dynamics. The study not only enhances the understanding of the underlying mechanisms but also identifies potential therapeutic targets within the astrocyte mitochondrial and histamine receptor pathways. These targets present opportunities for developing novel strategies to protect astrocytes from metabolic stress and improve neurological outcomes in diabetes-related conditions.

Our previous study found that the histidine metabolic status and HR systems in the hippocampus is highly responsive to glycemic fluctuations [8]. However, in conditions characterized by increased GV, the precise effects on astrocytes, as well as the mechanisms through which they regulate hippocampal energy metabolism, remain unclear. This study initially validated, through immunofluorescence co-localization, that increased GV can induce a decrease in HR expression in astrocytes within the mouse hippocampus. Conversely, histidine intervention was found to up-regulate its expression, with statistically significant effects observed for H_1R and H_3R. Furthermore, targeting metabolomics analysis unveiled alterations in energy metabolism pathways such as glycolysis, oxidative phosphorylation, and the TCA cycle in hippocampal tissue of mice experiencing increased GV compared to normal mice. Notably, while several key glycolytic metabolites were reduced, we observed elevated levels of Glucose-6-P and lactate under conditions of increased GV. This apparent discrepancy in glycolytic metabolites suggests a complex metabolic response to GV, potentially involving alternative pathways for lactate production. A previous study showed similar results in comparison with the diabetic group: metabolic pathways such as TCA cycle and gluconeogenesis were differentially altered in the hippocampus of diabetic rats exposed to recurrent hypoglycemia. Meanwhile, the activities of key glycolytic enzymes, such as hexokinase, phosphofructokinase, and pyruvate kinase, have also been compromised [25]. Although there are differences in the control groups of various

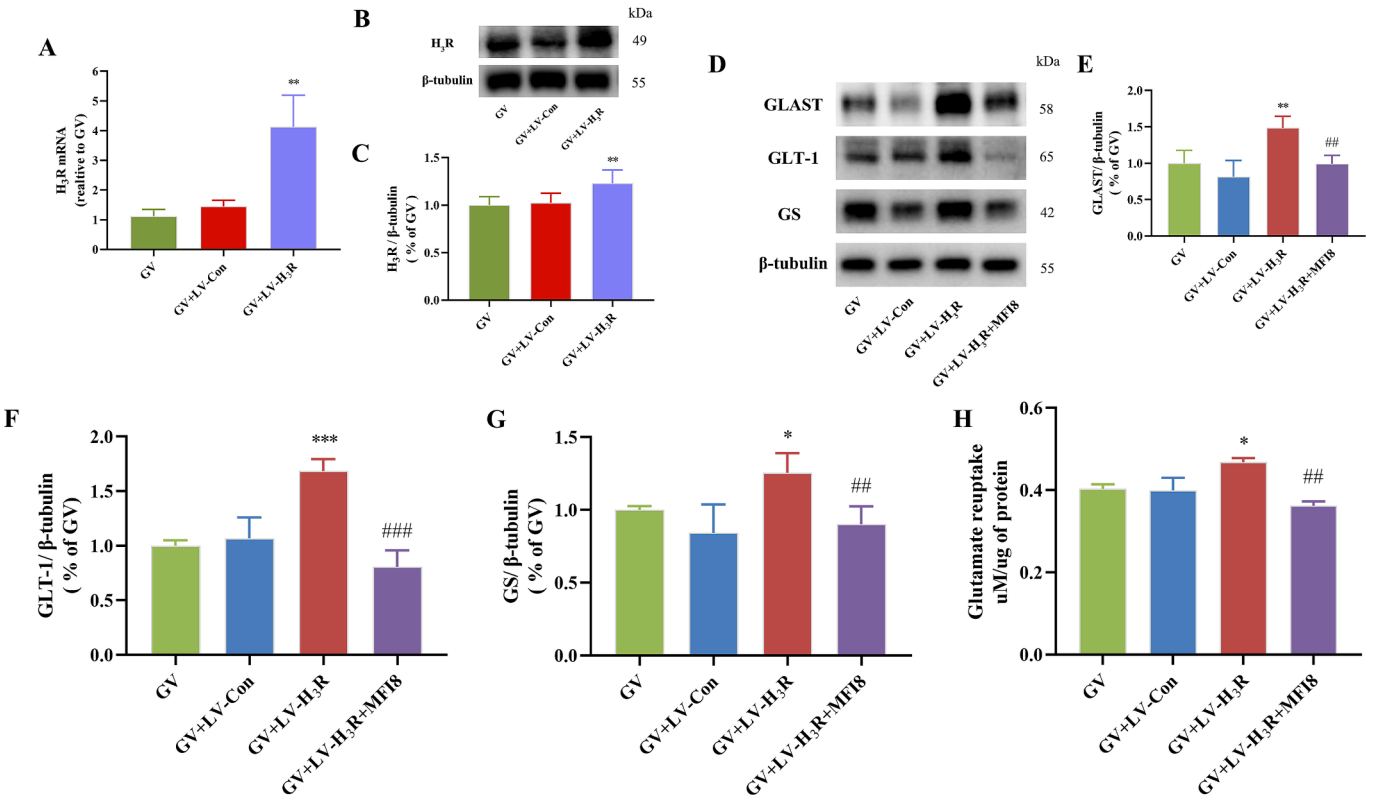

Fig. 7. H_3R balanced mitochondrial dynamics to restore the glutamate reuptake function of astrocytes in the context of high GV. (A) Transcription level of H_3R mRNA. (B) Representative immunoblot images of H_3R protein. (C) Relative protein levels of H_3R. (D) Representative immunoblot images of proteins associated with glutamate metabolic clearance. (E-G) Relative protein levels of GLAST, GLT-1 and GS. (H) Glutamate reuptake capacity. N = 6. * $P < 0.05$, ** $P < 0.01$, *** $P < 0.001$, GV + LV- H_3R vs. GV; ## $P < 0.01$, ### $P < 0.001$, GV + LV- H_3R + MFI8 vs. GV + LV- H_3R. GLAST, glutamate-aspartate transporter; GLT-1, glutamate transporter-1; GS, glutamine synthetase; H_3R, histamine receptor 3; H_3R, histamine receptor 3; GV + LV- Con, glucose variability + transfected empty vector lentivirus; GV + LV- H_3R, glucose variability + transfected H_3R lentivirus; GV + LV- H_3R + MFI8, glucose variability + transfected H_3R lentivirus + mitochondrial fusion inhibitor.

studies, these findings indirectly demonstrate that hippocampal energy metabolism is highly sensitive to changes in body glucose homeostasis, and different forms of changes in blood glucose homeostasis can trigger issues in hippocampal energy metabolism. In this study, we discovered the potential of histidine to improve the imbalance in hippocampal energy metabolism under conditions of high GV, as it can reverse the changes in the content of some metabolites in the aforementioned energy metabolic pathways. Interestingly, we observed increased levels of alanine in the GV group compared to the NC group, while glutamate and L-glutamine levels were elevated in the GV+ his group relative to the GV group. Lactate levels were increased in the GV group compared to the NC group and further elevated in the GV+ his group relative to the GV group. Additionally, NAD+ levels were decreased in the GV group compared to the NC group. These metabolic changes, particularly the elevated lactate levels despite apparent downregulation of some glycolytic metabolites, suggest an enhanced transamination process. This process could generate pyruvate (further converted to lactate) and glutamate (further converted to glutamine), providing an alternative explanation for the observed metabolic shifts under conditions of increased glucose variability and histidine intervention.

Our targeted metabolomics study captured these changes in glutamate metabolism, consistent with the observed changes in the expression of proteins related to glutamate metabolic clearance in the hippocampal area. In further in vitro studies, we observed that high GV significantly affected the expression of HRs (including H_1R, H_2R, and H_3R) and proteins related to glutamate metabolic clearance in primary astrocytes, with a reduced capacity for glutamate reuptake. Upon histamine intervention in these cells, the expression of all three HR subtypes was significantly increased, and the indicators related to glutamate metabolic clearance were reversed. However, when these three HR subtypes were inhibited pharmacologically, the glutamate reuptake capacity of primary astrocytes was again significantly reduced. This series of findings confirms that HRs play a critical role in regulating glutamate metabolic clearance function in astrocytes in states of increased GV. In addition, astrocytes from the GV group showed significant increases in glucose uptake and lactate secretion capacity compared to the normal group. However, these capacities did not demonstrate significant changes after histamine intervention. This phenomenon may indicate that the HR system could influence the regulation of glutamate metabolic clearance in astrocytes, possibly through the mitochondrial pathway, in an environment of increased glucose variability.

Research has shown that oxidative phosphorylation of mitochondria has been found to be not essential for bioenergy, proliferation and survival of astrocytes [26]. Nevertheless, mitochondria of astrocytes express all TCA cycle enzymes and maintain modest oxidative phosphorylation activity [27], suggesting that they assume other metabolic roles in addition to glucose oxidation and ATP production. For instance, moderate levels of oxidative phosphorylation activity in astrocytes are crucial for eliminating lipid waste products and safeguarding the brain from lipotoxicity and degeneration [28]. In this study, we found that under conditions of high GV, when HRs are inhibited, there are significant abnormalities in the mitochondrial function of astrocytes, including fragmentation, increased accumulation of ROS, decreased respiratory capacity, and imbalance in dynamics. Different HR subtypes differ in regulating mitochondrial function, particularly H_3R. Overexpression of H_3R reverses disturbances in mitochondrial dynamics, thereby restoring glutamate metabolic clearance in

astrocytes. These results confirm the key role of the mitochondrial pathway in the regulation of glutamate metabolic clearance by HRs in astrocytes. Additionally, they unveil the differential regulation of mitochondrial function by different HR subtypes. We believe that the potential reasons for this differential regulation may include the following aspects: 1) Differences in signaling pathways. It has been shown that different HR subtypes on astrocytes can modulate cellular function by activating different signaling pathways [18]. H_3R may regulate the expression or activity of proteins involved in mitochondrial dynamics through specific signaling pathways, such as cAMP or mitogen-activated protein kinase (MAPK) pathways, thereby having a more significant impact on mitochondrial function. 2) HR subtypes may differ in their distribution and localization within astrocytes. If a certain isoform (e.g., H_3R has a higher expression level or a more preferential localization near mitochondria, then its regulatory effect on mitochondrial function may be more direct and significant. 3) Differences in receptor activity or affinity. Astrocyte HR subtypes may differ in their binding activity or affinity to ligands (histamine). If H_3R has a higher affinity for histamine or a stronger activation effect, then it may mediate a more significant modulation of cellular responses and mitochondrial function. The mechanism of these differential regulation needs to be confirmed by further studies.

Our study has the following limitations: current research has primarily focused on brain damage caused by repeated hypoglycemia-induced GV, but the effects and mechanisms of glycemic fluctuations between high and normal levels in diabetic patients, as well as high GV in non-diabetic patients under conditions such as infections or tumors, and the influence of histamine and its receptors' regulatory roles, remain unclear. Additionally, our animal model used a chemically induced T1D mouse model, which may not fully simulate the specific human condition. Moreover, astrocytes exhibit transcriptomic and functional heterogeneity across different brain regions and even different cortical layers [9]. Therefore, it is crucial to further study the heterogeneity and mechanisms of action of astrocytes under conditions of high GV, which will help us more comprehensively understand how astrocytes respond under different metabolic states.

In summary, our study demonstrates that under conditions of increased GV, histamine and its receptors significantly impact the mitochondrial function and glutamate clearance ability of astrocytes. Particularly, the activation of H_3R can reverse the mitochondrial dysfunction and decline in glutamate clearance ability caused by increased GV, offering a new potential target for the treatment of diabetes-related cognitive decline.

Funding

This study was funded by the National Natural Science Foundation of China (No. 82100872 and 82200895), the High-level Personnel Research Start-up Funding of Fujian Medical University (No. XRCZX2020003).

CRediT authorship contribution statement

Yu Zhou: Writing – original draft, Project administration, Investigation, Funding acquisition. **Wenhuo Xie:** Writing – original draft, Validation, Project administration, Investigation. **Chenghua Kong:** Validation, Formal analysis. **Wei Luo:** Validation, Methodology. **Hong Wei:** Writing – review & editing, Supervision. **Jiaping Zheng:** Writing – review & editing, Supervision, Project administration.

Declaration of competing interest

The authors declare that they have no known competing financial interests or personal relationships that could have appeared to influence the work reported in this paper.

Acknowledgments

We thank the Public Technology Service Center (Fujian Medical University, China) for their assistance in the optical imaging analyses.

Data availability

Data will be made available on request.

References

[1] A. Ceriello, L. Monnier, D. Owens, Glycaemic variability in diabetes: clinical and therapeutic implications, The Lancet Diabetes & Endocrinology 7 (3) (2019) 221–230, https://doi.org/10.1016/s2213-8587(18)30136-0.
[2] A. Ceriello, Glucose Variability and Diabetic Complications: Is It Time to Treat? Diabetes Care 43 (6) (2020) 1169–1171, https://doi.org/10.2337/dci20-0012.
[3] F. Wang, M. Zhao, Z. Han, et al., Long-Term Subclinical Hyperglycemia and Hypoglycemia as Independent Risk Factors for Mild Cognitive Impairment in Elderly People, The Tohoku Journal of Experimental Medicine 242 (2) (2017) 121–128, https://doi.org/10.1620/tjem.242.121.
[4] M. Nilsson, N. Jensen, M. Gejl, et al., Experimental non-severe hypoglycaemia substantially impairs cognitive function in type 2 diabetes: a randomised crossover trial, Diabetologia 62 (10) (2019) 1948–1958, https://doi.org/10.1007/s00125-019-4964-4.
[5] C.H. Lin, W.H. Sheu, Hypoglycaemic episodes and risk of dementia in diabetes mellitus: 7-year follow-up study, Journal of Internal Medicine 273 (1) (2013) 102–110, https://doi.org/10.1111/joim.12000.
[6] B. Sun, Z. Luo, J. Zhou, Comprehensive elaboration of glycemic variability in diabetic macrovascular and microvascular complications, Cardiovascular Diabetology 20 (1) (2021) 9, https://doi.org/10.1186/s12933-020-01200-7.
[7] Y. Zhou, L. Huang, W. Zheng, et al., Recurrent nonsevere hypoglycemia exacerbates imbalance of mitochondrial homeostasis leading to synapse injury and cognitive deficit in diabetes, American Journal of Physiology Endocrinology and Metabolism 315 (5) (2018) E973–E986, https://doi.org/10.1152/ajpendo.00133.2018.
[8] K. Wu, W. Xie, Z. Chen, et al., Disturbed hippocampal histidine metabolism contributes to cognitive impairment induced by recurrent nonsevere hypoglycemia in diabetes, Biochemical and Biophysical Research Communications 682 (2023) 325–334, https://doi.org/10.1016/j.bbrc.2023.10.036.
[9] P. Hasel, S.A. Liddelow, Astrocytes, Curr Biol 31 (7) (2021) R326–R327, https://doi.org/10.1016/j.cub.2021.01.056.
[10] M. Santello, N. Toni, A. Volterra, Astrocyte function from information processing to cognition and cognitive impairment, Nature Neuroscience 22 (2) (2019) 154–166, https://doi.org/10.1038/s41593-018-0325-8.
[11] A. Joseph, R. Robinson, C.S. Paulose, Enhanced [3H] glutamate binding in the cerebellum of insulin-induced hypoglycaemic and streptozotocin-induced diabetic rats, Cellular and Molecular Neurobiology 27 (8) (2007) 1085–1095, https://doi.org/10.1007/s10571-007-9198-1.
[12] A. Joseph, S. Antony, C.S. Paulose, Increased glutamate receptor gene expression in the cerebral cortex of insulin induced hypoglycemic and streptozotocin-induced diabetic rats, Neuroscience 156 (2) (2008) 298–304, https://doi.org/10.1016/j.neuroscience.2008.07.022.
[13] R. Robinson, A. Krishnakumar, C.S. Paulose, Enhanced dopamine D1 and D2 receptor gene expression in the hippocampus of hypoglycaemic and diabetic rats, Cellular and Molecular Neurobiology 29 (3) (2009) 365–372, https://doi.org/10.1007/s10571-008-9328-4.
[14] J.V. Andersen, A. Schousboe, A. Verkhratsky, Astrocyte energy and neurotransmitter metabolism in Alzheimer's disease: Integration of the glutamate/GABA-glutamine cycle, Progress in Neurobiology 217 (2022) 102331, https://doi.org/10.1016/j.pneurobio.2022.102331.
[15] P.G. Weightman Potter, J.M. Vlachaki Walker, J.L. Robb, et al., Basal fatty acid oxidation increases after recurrent low glucose in human primary astrocytes, Diabetologia 62 (1) (2019) 187–198, https://doi.org/10.1007/s00125-018-4744-6.
[16] R. Gao, L. Ren, Y. Zhou, et al., Recurrent non-severe hypoglycemia aggravates cognitive decline in diabetes and induces mitochondrial dysfunction in cultured astrocytes, Molecular and Cellular Endocrinology 526 (2021) 111192, https://doi.org/10.1016/j.mce.2021.111192.
[17] J. Xu, X. Zhang, Q. Qian, et al., Histamine upregulates the expression of histamine receptors and increases the neuroprotective effect of astrocytes, Journal of Neuroinflammation 15 (1) (2018) 41, https://doi.org/10.1186/s12974-018-1068-x.
[18] D.M. Jurič, M. Kržan, M. Lipnik-Stangelj, Histamine and Astrocyte Function. Pharmacological Research 111 (2016) 774–783, https://doi.org/10.1016/j.phrs.2016.07.035.
[19] R. Gao, Z. Chen, Y. Wu, et al., SIRT3 alleviates mitochondrial dysfunction induced by recurrent low glucose and improves the supportive function of astrocytes to neurons, Free Radical Biology & Medicine 193 (Pt 1) (2022) 405–420, https://doi.org/10.1016/j.freeradbiomed.2022.10.313.
[20] Q. Fang, W.W. Hu, X.F. Wang, et al., Histamine up-regulates astrocytic glutamate transporter 1 and protects neurons against ischemic injury, Neuropharmacology 77 (2014) 156–166, https://doi.org/10.1016/j.neuropharm.2013.06.012.

[21] T. Masuoka, R. Ikeda, S. Konishi, Persistent activation of histamine H(1) receptors in the hippocampal CA1 region enhances NMDA receptor-mediated synaptic excitation and long-term potentiation in astrocyte- and D-serine-dependent manner, Neuropharmacology 151 (2019) 64–73, https://doi.org/10.1016/j.neuropharm.2019.03.036.

[22] F.M. Yakes, B. Van Houten, Mitochondrial DNA damage is more extensive and persists longer than nuclear DNA damage in human cells following oxidative stress, Proceedings of the National Academy of Sciences of the United States of America 94 (2) (1997) 514–519, https://doi.org/10.1073/pnas.94.2.514.

[23] D.C. Chan, Mitochondrial Dynamics and Its Involvement in Disease, Annual Review of Pathology 15 (2020) 235–259, https://doi.org/10.1146/annurev-pathmechdis-012419-032711.

[24] E. Zacharioudakis, B. Agianian, V. Kumar Mv, et al., Modulating mitofusins to control mitochondrial function and signaling, Nature Communications 13 (1) (2022) 3775, https://doi.org/10.1038/s41467-022-31324-1.

[25] N. Dewan, V. Shukla, A.K. Rehni, et al., Exposure to recurrent hypoglycemia alters hippocampal metabolism in treated streptozotocin-induced diabetic rats, CNS Neuroscience & Therapeutics 26 (1) (2020) 126–135, https://doi.org/10.1111/cns.13186.

[26] G. Bonvento, J.P. Bolaños, Astrocyte-neuron metabolic cooperation shapes brain activity, Cell Metabolism 33 (8) (2021) 1546–1564, https://doi.org/10.1016/j.cmet.2021.07.006.

[27] I. Lopez-Fabuel, J. Le Douce, A. Logan, et al., Complex I assembly into supercomplexes determines differential mitochondrial ROS production in neurons and astrocytes, Proceedings of the National Academy of Sciences of the United States of America 113 (46) (2016) 13063–13068, https://doi.org/10.1073/pnas.1613701113.

[28] Y. Mi, G. Qi, F. Vitali, et al., Loss of fatty acid degradation by astrocytic mitochondria triggers neuroinflammation and neurodegeneration, Nature Metabolism 5 (3) (2023) 445–465, https://doi.org/10.1038/s42255-023-00756-4.